J. Phys. Res. Edu., Vol. 1, March 2024

A short course on the Su-Schrieffer-Heeger model

Tarun Kanti Ghosh*

Department of Physics, Indian Institute of Technology-Kanpur, Kanpur-208 016, India

We review various topological properties of a dimer Su-Schrieffer-Heeger tight-binding model. Exact analytical expressions of the energy spectrum and corresponding eigenstates for any choice of system parameters are provided. We discuss the system's parity, time-reversal, and chiral symmetries. The system undergoes a topological phase transition while tuning the hopping parameters. The topological phase is associated with the presence of the boundary modes and establishes the bulk-boundary correspondence.

I. INTRODUCTION

One of the successful applications of early quantum mechanics is the band theory of crystallne materials [1]. The superposition of the Bloch states leads to the formation of well separated energy bands. The crystalline materials can be classified into two categories, namely the insulator and the metal, depending on whether the bands are completely or partially filled. Completely filled bands are well separated from the completely empty bands in a band insulator. The energy gap prohibits the flow of the charge carriers in the band insulator. On the other hand, materials having partially filled bands are conductors, where charge carriers can easily flow at the cost of very low energy.

After the phenomenal discovery of the integer quantum Hall effect [2] in early 1980s, the simple concept of the band insulator has changed. In the integer quantum Hall effect, a strong perpendicular magnetic field freezes the electron's motion in the bulk of a two-dimensional (2D) semiconductor but the edge states at the boundary conducts current. Thus, a 2D system subjected to a strong magnetic field behaves like an insulator in the bulk and metallic at the boundaries, by forming a discrete number of edge states. The number of edge states is directly related to the topological invariant of the bulk bands, namely the Chern number.

Over the last few decades, it has been established that the nontrivial topology of the bulk bands gives rise to the conducting edge states in the insulating materials. Such systems are usually called as the topological material/insulator [3–6]. Generally a topological phase transition may take place if a band gap closes and then reappears again as we change the parameter(s) of the system continuously while preserving the internal symmetry. The simplest topological system is an one-dimensional (1D) tight-binding dimer chain with alternating hopping parameters known as the Su-Schrieffer-Heeger (SSH) model [7]. Polyacetylene, a 1D

long polymer having large number of -CH- monomers, can be modeled by the tight-binding Hamiltonian of the SSH model. The SSH model is the simplest model to understand band topology, edge states, and bulk-boundary correspondence in 1D lattice systems. This would help us to understand more topological phenomena in higher dimensions. For example, the zero-energy edge states of the SSH model generalizes into 1D edge states of 2D topological insulators, and surface states of three-dimensional (3D) topological insulators, although the bulk-edge correspondence properties may differ. The topological phase of a finite system is manifested by the presence of exponentially localized zero-energy edge states.

The Zak phase [8] similar to the Berry phase [9] and the winding number have been used as a topological invariant quantity to classify various inversion-symmetric 1D topological systems. The Zak phase is quantized to π or 0 (mod 2π), whereas the winding number is either 1 or 0 [10]. The existence of the edge states and the Zak phase are confirmed in various artificial 1D systems such as cold atomic gases in optical lattices [11], photonic crystals [12, 13] and acoustic crystals [14].

This article is organized as follows. In Sec. II, we discuss some basic symmetry properties and bulk band structure of the SSH model Hamiltonian. The topological phase transition and bulk-boundary correspondence are discussed in Sec. III. In Sec. IV, we summarize the results. In Appendix A, we present alternative Bloch Hamiltonian for the SSH model.

II. SSH MODEL

The SSH model is described by the following nearest-neighbour (NN) tight-binding Hamiltonian

$$H = v\sum_{j=1}^{N}(a_j^\dagger b_j + b_j^\dagger a_j) + w\sum_{j=1}^{N-1}(a_{j+1}^\dagger b_j + b_j^\dagger a_{j+1}), \tag{1}$$

where $a_j^\dagger(a_j)$ and $b_j^\dagger(b_j)$ are the creation (annihilation) operator defined at the sub-lattice sites A and B, respectively in the j-th unit cell (Fig. 1). In the present case the nearest-neighbour (NN) real hopping parameters v and w may be called intra-cell and inter-cell hopping amplitudes, respectively. We will discuss

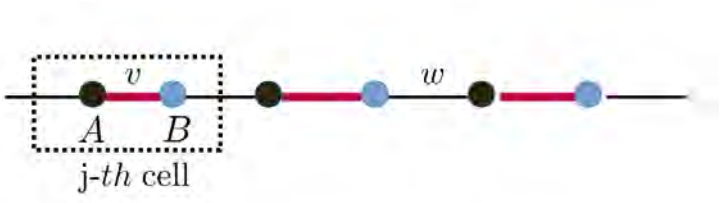

FIG. 1: Schematic diagram of the dimer SSH model. The unit cell of length a is depicted by the dotted rectangle contains two sub-lattices A and B.

some basic properties of the Bloch Hamiltonian of the SSH model. There are mainly two representations of the Bloch Hamiltonian depending on the two distinct choices of the basis states: the periodic Bloch Hamiltonian and the canonical Bloch Hamiltonian. Both the representations are useful and convenient to study certain topological aspects of the systems. We proceed with the periodic Bloch Hamiltonian. The derivation of the canonical Bloch Hamiltonian is provided in Appendix A.

A. Periodic Bloch Hamiltonian

As the system is translationally invariant, we can diagonalize the Hamiltonian using the cell index j. We expand the real space field operators defined at the sites A and B in the j-th cell

$$a_j = \frac{1}{\sqrt{N}} \sum_{k \in BZ} e^{ikaj} a_k,\ b_j = \frac{1}{\sqrt{N}} \sum_{k \in BZ} e^{ikaj} b_k, \tag{2}$$

where k is the crystal wave vector lying within the first Brillouin zone (BZ) ($-\pi$ to π), N is the number of unit cells, a is the length of the unit cell and $a/2$ is the spacing between two successive sites. Using

$$\sum_{j=1}^{N} e^{i(k-k')ja} = N\delta_{k,k'}, \tag{3}$$

the Hamiltonian in Eq. (1) reduces to the following form

$$H = v\sum_k (a_k^\dagger b_k + b_k^\dagger a_k) + w\sum_k (e^{ika} a_k^\dagger b_k + e^{-ika} b_k^\dagger a_k) = \sum_k \psi_k^\dagger \mathcal{H}(k) \psi_k, \tag{4}$$

where the spinor $\psi_k^\dagger = (a_k^\dagger, b_k^\dagger)$. Here, $\mathcal{H}(k)$ is given by

$$\mathcal{H}(k) = \begin{pmatrix} 0 & v + we^{-ika} \\ v + we^{ika} & 0 \end{pmatrix} = \begin{pmatrix} 0 & h_x(k) - ih_y(k) \\ h_x(k) + ih_y(k) & 0 \end{pmatrix} \tag{5}$$

with $h_x(k) = v + w\cos(ka)$ and $h_y(k) = w\sin(ka)$. Note that $\mathcal{H}(k)$ can be expressed in terms of the Pauli matrices (σ_x, σ_y) as

$$\mathcal{H}(k) = \boldsymbol{\sigma} \cdot \boldsymbol{h}(k), \tag{6}$$

where $\boldsymbol{h}(k)$ is $\boldsymbol{h}(k) = h_x(k)\hat{i} + h_y(k)\hat{j}$. The Pauli matrices $\boldsymbol{\sigma}$ do not represent the real spin of the fermions, they act on the sublattice sites (A, B). In real space, the SSH Hamiltonian is a $2N \times 2N$ matrix, whereas it becomes a 2×2 matrix $\mathcal{H}(k)$ for each value of k. This Hamiltonian $\mathcal{H}(k)$ is periodic in k with periodicity $2\pi/a$: $\mathcal{H}(k + 2\pi/a) = \mathcal{H}(k)$ due to the fact that only the cell index j is used to perform the Fourier transformation of the real space Hamiltonian.

Interestingly, the periodic Hamiltonian $\mathcal{H}(k)$ has the same structure as that of a spin-1/2 particle in an in-plane rotating magnetic field. Here, $\boldsymbol{h}(k)$ plays the role of the in-plane rotating magnetic field and the two sublattices A and B play the roles of spin-up and spin-down components. Therefore, the Zak phase due to variation of the parameter k equals half of the solid angle extended by a closed path in the $\boldsymbol{h}$-space.

B. Symmetry properties of the SSH model Hamiltonian

In this sub-section, we shall discuss some of basic symmetries of the Bloch Hamiltonian.

Space-inversion symmetry: The space-inversion symmetry is equivalent to the reflection symmetry. Considering the mid-point between the two sublattices A and B as the center of space-inversion and its operation simply exchanges the two sublattices. Then the space inversion operator in the pseudospin space can be simply written as σ_x. Under the space-inversion operation, the coordinates in phase space transform as $x \to -x$ and $k \to -k$. Further, $h_x(-k) = h_x(k)$ and $h_y(-k) = -h_y(k)$. Therefore, under the space inversion operation

$$\mathcal{P}\mathcal{H}(k)\mathcal{P} = \sigma_x \mathcal{H}(-k)\sigma_x = \mathcal{H}(k). \tag{7}$$

Here we have used $\sigma_x\sigma_y = -\sigma_y\sigma_x$. Thus, the Hamiltonian $\mathcal{H}(k)$ is invariant under the space-inversion with respect to the mid-point of the two sublattices.

Time-reversal symmetry: As the Pauli matrices do not represent the real spin of the charge carrier, the time-reversal operator $\mathcal{T}$ for a spinless fermion is simply $\mathcal{T} = \mathcal{C}$, with $\mathcal{C}$ being the complex conjugation operator, along with $k \to -k$. Note that $\mathcal{C}\sigma_y\mathcal{C} = -\sigma_y$ and the remaining Pauli matrices are even under time-reversal operation. Under the time-reversal operation,

$$\mathcal{T}\mathcal{H}(k)\mathcal{T} = \mathcal{C}\mathcal{H}(-k)\mathcal{C} = \mathcal{H}(k). \tag{8}$$

Therefore, the SSH Hamiltonian is invariant under time-reversal operation.

Chiral symmetry: The chiral symmetry, also known as sublattice symmetry, states that if there is a state u_k with energy $E(k)$ for a given Hamiltonian $H(k)$, there must be a state $\mathcal{S}u_k$ with energy $-E(k)$, with $\mathcal{S}$ being the chiral operator. Mathematically, it can be written as $\mathcal{S}H(k)\mathcal{S} = -H(k)$, or $H(k)\mathcal{S} = -\mathcal{S}H(k)$. The spectrum is symmetric around zero energy of a chiral symmetric Hamiltonian which explains the particle-hole symmetry. In the present case, it can be easily checked that $\sigma_z\mathcal{H}(k)\sigma_z = -\mathcal{H}(k)$. Therefore σ_z is identified as the chiral operator and the system has a chiral symmetry. The chiral symmetry will be lost if σ_z is present in the Hamiltonian $\mathcal{H}(k)$. The absence of σ_z arises due to $h_z(k) = 0$. Therefore, the chiral symmetry enforces the vector $\boldsymbol{h}(k)$ to lie on the equator plane of the Bloch sphere.

The periodic Bloch Hamiltonian $\mathcal{H}(k)$ and its eigenstates (discussed below) for each k are expressed in terms of the unit vector $\hat{\boldsymbol{h}}(k) = \boldsymbol{h}(k)/|\boldsymbol{h}(k)|$ on the equator of the Bloch sphere. The BZ of 1D lattice structure has the shape of a circle since the eigenstates at the two end-points ($k = \pm\pi$) of the BZ are equivalent. At the same time, the tip of the unit vector $\hat{\boldsymbol{h}}(k)$ traces a circle on the equator of the Bloch sphere while k runs across the BZ. The mapping of the circular BZ to the circle on the equator traced by $\hat{\boldsymbol{h}}(k)$ allows us to define a winding number ν of $\boldsymbol{h}(k)$ around the origin. Thus, the winding number ν is protected by the chiral symmetry.

There is an ambiguity of labelling $\nu = 0$ or $\nu = 1$ to trivial phase or non-trivial phase. For an infinite system, we can not determine whether the system is in trivial phase or non-trivial phase based on integer values of ν since the unit cell can be chosen in two different ways. There is no ambiguity if the changes in the winding number is $\Delta\nu = \pm 1$ while going from one phase to another phase. There is no ambiguity for finite chain since the unit cell can be chosen uniquely.

The sublattice symmetry operator can be written in terms of the sub-lattice projection operators P_α of each sub-lattice $\alpha = A, B$ as $\mathcal{S} = P_A - P_B$, where the projection operators are

$$P_A = |A\rangle\langle A| = \begin{pmatrix} 0 & 1 \\ 0 & 0 \end{pmatrix} \text{ and } P_B = |B\rangle\langle B| = \begin{pmatrix} 0 & 0 \\ 1 & 0 \end{pmatrix}. \tag{9}$$

C. Energy bands, eigenstates and their properties

We obtain the energy band structure of the SSH model, by diagonalizing the Hamiltonian $\mathcal{H}(k)$, as

$$E_\pm(k) \;=\; \pm|\boldsymbol{h}(k)| = \pm\sqrt{v^2 + w^2 + 2vw\cos(ka)}. \tag{10}$$

The energy bands are symmetric around zero energy axis since the chiral symmetry is preserved. Further, the energy bands are symmetric in k, $E_\pm(-k) = E_\pm(k)$, due to the space inversion symmetry. The maximum bandwidth at the Γ-point ($k = 0$) is $2(v + w)$. The two energy bands satisfy following relations: (i) $E_+(k) + E_-(k) = 0$ as expected since trace of the Hamiltonian $\mathcal{H}(k)$ is zero and (ii) $E_+^2(k) + E_-^2(k) = 2|\boldsymbol{h}(k)|^2$, describing a circle of radius $\sqrt{2}|\boldsymbol{h}(k)|$ centered at origin.

Figure 2 displays the band dispersion for various parameters. For staggered hopping parameters, $v \neq w$ (see left and right panels of Fig. 2), there is a minimum energy gap $E_g = E_+(k) - E_-(k) = 2|w - v|$ at $k = \pm\pi/a$. On the other hand, the gap E_g closes at $k = \pm\pi/a$ when $v = w$, which is equivalent to a monatomic chain of lattice constant $a/2$ with the metallic dispersion $E(k) = 2t\cos(ka/2)$. Therefore, staggered hopping parameters are required in order to open a gap in the dispersion. Moreover, the gap closing at $v = w$ indicates a topological phase transition.

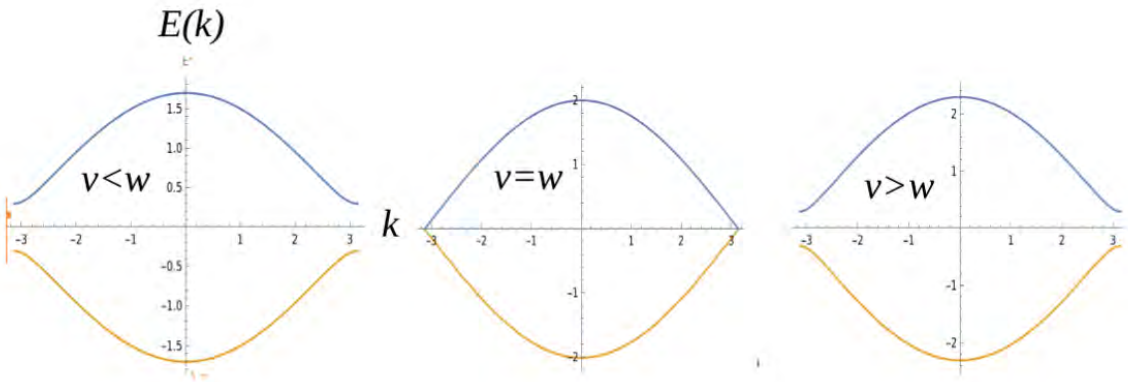

FIG. 2: Energy band dispersion: Left panel: $v = 0.7, w = 1$, Middle panel: $v = w = 1$, Right panel: $v = 1.3, w = 1$.

The eigenspinors of $\mathcal{H}(k)$ located on the equator of the Bloch sphere are given by

$$u_+(k) = \frac{1}{\sqrt{2}} \begin{pmatrix} 1 \\ e^{i\gamma_k} \end{pmatrix} \quad \text{and} \quad u_-(k) = \frac{1}{\sqrt{2}} \begin{pmatrix} 1 \\ -e^{i\gamma_k} \end{pmatrix} \tag{11}$$

with the phase angle $\gamma_k = \arctan(h_y/h_x)$ in the h_x-h_y plane on the equator of the Bloch sphere. Both the eigenspinors are well-defined for all values of k with $v \neq w$. Note that $u_-(k) = \sigma_z u_+(k)$ as expected from the chiral symmetry.

Let us first rewrite the band dispersion $E_\pm(k)$ in terms of $z = \delta/(2t)$ with $t = (v+w)/2$ and $\delta = w - v$ as

$$E_\pm(k) \;=\; \pm 2t\sqrt{1 - (1 - z^2)\sin^2(ka/2)}. \tag{12}$$

This form of $E_\pm(k)$ will be convenient to study the group velocity, density of states and effective mass.

The group velocity can be obtained as

$$v_g = \frac{1}{\hbar}\frac{dE}{dk} \;=\; \frac{at}{\hbar}\frac{(z^2-1)\sin(ka)}{\sqrt{1 - (1 - z^2)\sin^2(ka/2)}}. \tag{13}$$

Total number of states per unit length in one-dimension is $N(k) = k/\pi$. The density of states is then given by

$$\frac{dN(k)}{dE} = \frac{1}{\pi}\frac{dk}{dE}.$$

The density of states of either bands for the spinless fermions can be obtained as

$$D(E) = \frac{1}{\pi}\frac{dk}{dE} = \frac{1}{\pi a}\frac{|E|}{\sqrt{(4t^2 - E^2)(E^2 - \delta^2)}}. \tag{14}$$

The density of states has Van Hove singularity at $E = \delta$ and at $E = 2t$. There is no available density of states in the gap region $-\delta < E < \delta$.

Limiting case: Note that when $\delta = 0$, the lattice is equivalent to a monatomic chain of lattice constant $a/2$ with the dispersion $E = 2t\cos(ka/2)$. The BZ is now $-2\pi/a \leq k \leq 2\pi/a$. The band minimum ($E_{min} = -2t$) occurs at $k = \pm 2\pi/a$ and maximum $E_{max} = 2t$ at $k = 0$.

In this case ($z = 0$), the group velocity becomes $v_g = -(at/\hbar)\sin(ka/2)$. The density of states correctly reproduces to

$$D(E) = \frac{1}{\pi a}\frac{1}{\sqrt{(4t^2 - E^2)}}. \tag{15}$$

III. BULK AND EDGE STATES OF A FINITE SSH MODEL

The SSH model supports the bulk as well as the edge states. In the previous Section, we have discussed properties of the bulk bands for an infinite SSH chain. The difference between the bulk and the edge states is characterized by the spreading of energy eigenstates in the real space. Now we shall consider a finite chain and study both the bulk and the edge states by diagonalizing the Hamiltonian in Eq. 1 in real space. As an example, here we provide the matrix eigenvalue equation, $H\Psi = E\Psi$, for 4 unit cells as given by

$$H\Psi = \begin{pmatrix} 0 & v & 0 & 0 & 0 & 0 & 0 & 0 \\ v & 0 & w & 0 & 0 & 0 & 0 & 0 \\ 0 & w & 0 & v & 0 & 0 & 0 & 0 \\ 0 & 0 & v & 0 & w & 0 & 0 & 0 \\ 0 & 0 & 0 & w & 0 & v & 0 & 0 \\ 0 & 0 & 0 & 0 & v & 0 & w & 0 \\ 0 & 0 & 0 & 0 & 0 & w & 0 & v \\ 0 & 0 & 0 & 0 & 0 & 0 & v & 0 \end{pmatrix} \begin{pmatrix} a_1 \\ b_1 \\ a_2 \\ b_2 \\ a_3 \\ b_3 \\ a_4 \\ b_4 \end{pmatrix} = E \begin{pmatrix} a_1 \\ b_1 \\ a_2 \\ b_2 \\ a_3 \\ b_3 \\ a_4 \\ b_4 \end{pmatrix}. \tag{16}$$

Here, the eigenvector for four unit cells is $\Psi = (a_1, b_1, a_2, b_2, a_3, b_3, a_4, b_4)^T$ with the subscript in (a_j, b_j) denotes the cell index and T denotes the transpose. One can easily extend the matrix eigenvalue equations for an arbitrary N cells and solve the eigenvalue problem for all $2N$ discrete eigenvalues E as well as the corresponding real space eigenvectors.

Figures 3(a) and 3(b) display the spectrum of a finite SSH model of $N = 12$ and $N = 25$ unit cells considering the open boundary condition, while varying v for fixed $w = 1$. A careful analysis of the dispersion reveals that there are two nearly zero-energy states within the bulk band gap when $v < w$. The eigenvectors of the zero-energy edge states for $v = 0.2$ in the form of symmetric and anti-symmetric pairs (blue dot for $N = 12$) are shown in Figs. 3(c) and 3(d). Only the sub-lattice A at the left edge and the

sub-lattice B at the right edge are occupied. The amplitude of the eigenvectors inside the lattice is simply zero, thus the eigenvectors are exponentially localized.

The amplitude of the eigenvectors begins to spread inside the lattice and the bulk band gap shrinks to zero as v approaches to w. Similar to the previous case, two eigenvectors of the nearly-zero-energy edge states at $v = 0.7$ (maroon dot for $N = 12$) are shown in Figs. 3(e) and 3(f). It shows that amplitude of the eigenvectors become finite inside the lattice, giving rise to splitting in the energy levels. The edge state energies for $N = 12$ case start splitting earlier than that of the $N = 25$ case, due to the finite size effects.

There is no edge states within the bulk gap when $v > w$. The eigenvectors for $v = 2.5$ (red dots for $N = 12$) are shown in Figs. 3(e) and 3(f). The eigenvector profile of the bulk modes looks like a standing wave on the chain.

For $v < w$, only A sub-lattices are occupied at left half of the lattice, whereas B sub-lattices are occupied at right-half of the lattice. On the other hand, both the sub-lattices are occupied across the lattice for $v > w$ case. These zero-energy states localized at the edges are responsible for the topological phase for $v < w$ case. This phase can be characterized by the topological invariants, namely, the Zak phase and the winding number.

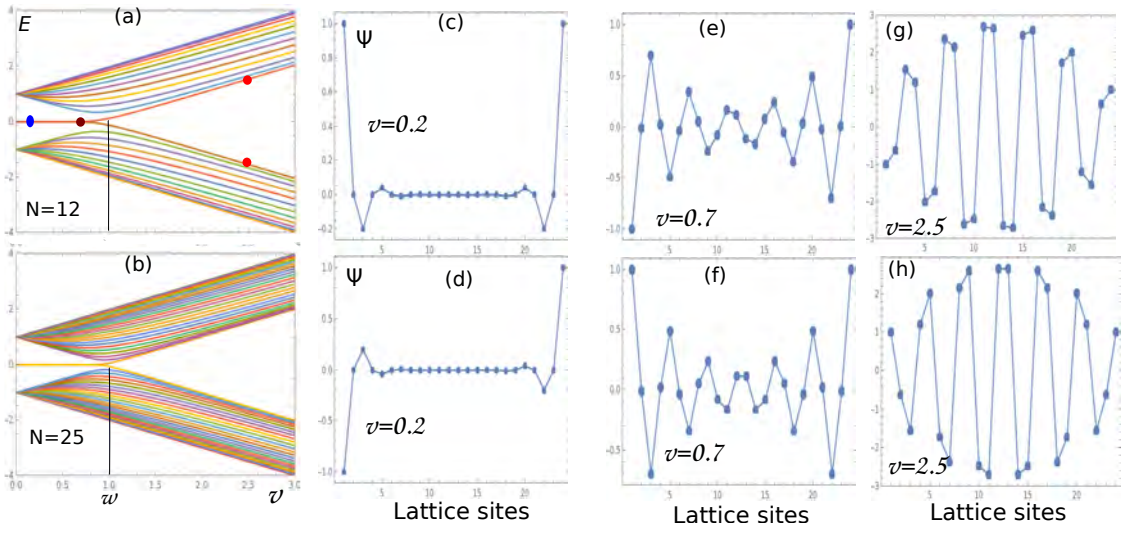

FIG. 3: Bulk bands and edge states of the finite SSH model in the open boundary condition, as a function v for fixed $w = 1$. Second, third and fourth panels show the eigenvectors of the hybridized states for various values of v.

A. Space inversion symmetry and sub-lattice symmetry operator for finite SSH Hamiltonian

Like the space inversion symmetry operator for bulk Hamiltonian, one can also construct the same for the finite SSH Hamiltonian. It is given by I = off-diag(1, 1,.....)$_{2N}$, satisfying the relation $IHI = H$.

The sub-lattice operator for the finite SSH Hamiltonian can be written as $\Sigma = P_A - P_B$, where the sub-lattice projection operators for the finite system are $P_A = \sum_{j=1}^{N} |j, A\rangle\langle j, A|$ and $P_B = \sum_{j=1}^{N} |j, B\rangle\langle j, B|$. For $N = 2$, the sub-lattice symmetry operator can be expressed in matrix form as

$$\Sigma = \begin{pmatrix} 1 & 0 & 0 & 0 \\ 0 & -1 & 0 & 0 \\ 0 & 0 & 1 & 0 \\ 0 & 0 & 0 & -1 \end{pmatrix}. \tag{17}$$

It can be easily checked that $\Sigma H \Sigma = -H$.

B. Approximate expression of the zero-energy eigenstates

The SSH Hamiltonian is

$$\mathcal{H} = [v + w\cos(ka)]\sigma_x + w\sin(ka)\sigma_y. \tag{18}$$

Expanding $\cos(ka)$ and $\sin(ka)$ around the gap closing points $ka = \pm\pi$ as $ka = \pm\pi + qa$, and keeping upto linear in qa, we get the low-energy Hamiltonian around the gap closing point as

$$\mathcal{H} \simeq (v - w)\sigma_x - wqa\sigma_y. \tag{19}$$

Setting $q \to -i\partial_x$, the Hamiltonian in real space reads as

$$\mathcal{H} = (v - w)\sigma_x + iwa\sigma_y\partial_x. \tag{20}$$

Let us see if there is any zero-energy edge state under certain conditions or not. The zero-energy eigenvalue equation can be written as

$$[(v - w)\sigma_x + iwa\sigma_y\partial_x]\psi(x) = 0, \tag{21}$$

where $\psi(x)$ is the zero-energy eigenstate. Multiplying σ_y, we get

$$\sigma_0\partial_x\psi(x) \;=\; \frac{(v - w)}{wa}\sigma_z\psi(x), \tag{22}$$

where σ_0 is the 2×2 identity matrix.

Consider a finite SSH chain of length $L = Na$ with N number of unit cells and the left end is at $x = 0$. Now, we substitute the following ansatz in the above equation, which will satisfy the boundary condition at $x = L$

$$\psi_r(x) = \begin{pmatrix} 0 \\ 1 \end{pmatrix} \phi_r(x).$$

The first-order differential equation for $\phi_r(x)$ has the solution

$$\phi_r(x) = e^{\frac{(v-w)}{wa}(L-x)}. \tag{23}$$

It clearly shows that the condition, $w > v$, must be satisfied in order to get a normalizable solution. Thus the zero-energy (unnormalized) eigenstate at the right edge is

$$\phi_r(x < L) = e^{-\frac{(w-v)}{wa}(L-x)}, \tag{24}$$

with $w > v$. Similarly, the zero-energy (unnormalized) eigenstate at the left edge can be obtained as

$$\psi_l(x > 0) = \begin{pmatrix} 1 \\ 0 \end{pmatrix} e^{-\frac{(w-v)}{wa}x}, \tag{25}$$

with $v < w$.

Both the eigenstates $\psi_l(x)$ and $\psi_r(x)$ are exponentially decaying functions with the decay length $\xi_c = wa/(w-v)$. The decay length decreases with the increase of $(w-v)$. Further, the spinor parts of $\psi_l(x)$ and $\psi_r(x)$ show that sublattice A at the left edge and the sublattice B at the right edge support a zero-energy state.

IV. BAND GEOMETRIC QUANTITIES AND BULK TOPOLOGICAL INVARIANT

The Berry connection for $E_-(k)$ band is

$$A_-(k) = i\langle u_-(k)|\partial_k u_-(k)\rangle = \frac{1}{2}\frac{d\gamma_k}{dk}. \tag{26}$$

The Zak phase acquired which is while traveling along a closed path in BZ is given by

$$Z_- = \int_{BZ} A_-(k)dk = \frac{1}{2}\oint_{BZ} d\gamma_k. \tag{27}$$

A care must be taken while calculating the above integral of the phase angle γ_k in $\boldsymbol{h}(k)$-space for two different cases: $v < w$ and $v > w$. Note that $h_x(k) = v + w\cos(ka)$ and $h_y(k) = w\sin(ka)$ parameterize a circle. When we vary k across the first BZ, the tip of $\boldsymbol{h}(k)$ sketches a circle of radius w whose center is

at v in the h_x-h_y plane as shown in Fig. 4. The gap closing points $ka = \pm\pi$ for $v = w$ correspond to the origin of the h_x-h_y plane. When $w > v$, the trajectory of $\boldsymbol{h}$ encloses the origin when k varies across the first BZ. Therefore, $\oint_{BZ} d\gamma_k = 2\pi$ and so the Zak phase is π. When $w < v$, the trajectory of the vector $\boldsymbol{h}$ excludes the origin, which leads to $\oint_{BZ} d\gamma_k = 0$ and so the Zak phase for this path is simply zero. The Zak phase for different cases can be written as

$$Z_- = \begin{cases} \pi & v < w \text{ (topological insulator)} \\ 0 & v > w \text{ (band insulator)} \end{cases} \tag{28}$$

The topology of this kind of closed loop can also be characterized by an integer, the bulk winding number ν. This counts the number of times the loop winds around the origin of the h_x-h_y plane. We have $\nu = 0$ when $w < v$, $\nu = 1$ when $w > v$ and ν is undefined when $w = v$ since the loop passes through the origin.

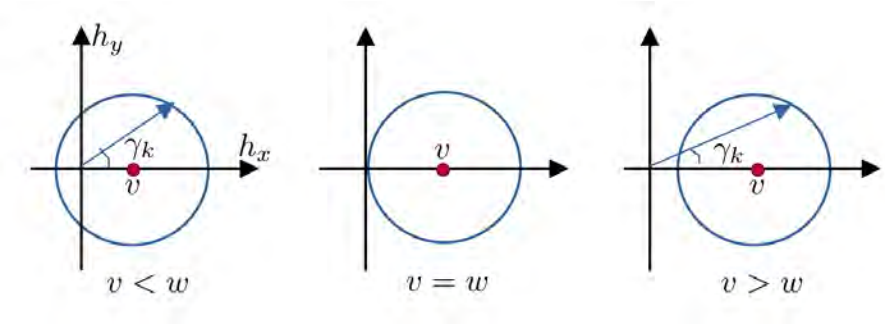

FIG. 4: Sketch of the trajectory of the tip of the $\boldsymbol{h}(k)$ vector while k varies in the first BZ for different choices of the hopping energies v and w.

Electric polarization: The electric polarization is created due to spatially separated charges. The electric polarization at k of a given band can be defined as

$$P_n(k) = e\langle x\rangle = ie\langle\partial_k\rangle. \tag{29}$$

The total polarization is the sum over all the occupied states in a given band

$$P_n = \frac{e}{2\pi}\oint P_n(k)dk = \frac{e}{2\pi}\oint i\langle\partial_k\rangle dk = \frac{e}{2\pi}\oint A(k)dk = \frac{e}{2\pi}Z_n. \tag{30}$$

Therefore, the electric polarization P is given by

$$P = \frac{e}{2\pi}\oint_{BZ} A(k)dk \tag{31}$$

$$= \begin{cases} \frac{e}{2}, & v < w \\ 0 & v > w. \end{cases} . \tag{32}$$

V. SUMMARY

In this article, we have discussed some interesting topological properties of the dimer SSH model. Various symmetries like the parity, the time-reversal and the chiral symmetries of the bulk Hamiltonian are also mentioned. We provide exact analytical expressions of the bulk band structures and corresponding eigenstates. The appearance of the boundary modes is shown by studying a finite SSH chain and establishing the bulk-boundary correspondence.

APPENDIX A: CANONICAL BLOCH HAMILTONIAN

In order to get the canonical Bloch Hamiltonian from the real space Hamiltonian given in Eq. (1), we use the Fourier transformation

$$a_j = \frac{1}{\sqrt{N}} \sum_k e^{ikaj} a_k,\ b_j = \frac{1}{\sqrt{N}} \sum_k e^{ika(j+1/2)} b_k. \tag{33}$$

The real space Hamiltonian H reduces to the form

$$H = v \sum_k (e^{ika/2} a_k^\dagger b_k + e^{-ika/2} b_k^\dagger a_k) + w \sum_k (e^{-ika/2} a_k^\dagger b_k + e^{ika/2} b_k^\dagger a_k) \tag{34}$$

$$= \sum_k \psi_k^\dagger H(k) \psi_k, \tag{35}$$

where $\psi_k^\dagger = (a_k^\dagger, b_k^\dagger)$. Here, the Hamiltonian $H(k)$ is given by

$$H(k) = \begin{pmatrix} 0 & d_x(k) - id_y(k) \\ d_x(k) + id_y(k) & 0 \end{pmatrix} \tag{36}$$

with $d_x(k) = (v + w)\cos(ka/2)$ and $d_y(k) = (w - v)\sin(ka/2)$. The canonical Bloch Hamiltonian can be further written as

$$H(k) = \boldsymbol{\sigma} \cdot \boldsymbol{d}(k), \tag{37}$$

where $\boldsymbol{d}(k) = \hat{i} d_x(k) + \hat{j} d_y(k)$.

Note that the periodicity of the Bloch Hamiltonian has increased by two times: $H(k + 4\pi/a) = H(k)$ because the separation distance between the sites in a given unit cell becomes half of the size of the unit cell. It is noteworthy that the canonical Bloch Hamiltonian $H(k)$ is directly obtained from the periodic Bloch Hamiltonian $\mathcal{H}(k)$ via the unitary transformation: $H(k) = U\mathcal{H}(k)U^\dagger$, where the unitary matrix U is given by $U = \text{diag}(1, e^{ika})$.

As expected, the energy dispersion is given by

$$E_{\pm}(k) \;=\; \pm|\boldsymbol{d}(k)| = \pm\sqrt{v^2 + w^2 + 2vw\cos(ka)}. \tag{38}$$

The eigenspinors for the canonical Bloch Hamiltonian $H(k)$ located on the equator of the Bloch sphere are

$$u_{+}(k) = \frac{1}{\sqrt{2}}\begin{pmatrix} 1 \\ e^{i\phi_k} \end{pmatrix}, \qquad u_{-}(k) = \frac{1}{\sqrt{2}}\begin{pmatrix} 1 \\ -e^{i\phi_k} \end{pmatrix}, \tag{39}$$

where $\phi_k = \arctan[d_y(k)/d_x(k)]$. The eigenspinors are not single-valued and ill-defined at $k = \pm\pi/a$.

---

* Electronic address: tkghosh@iitk.ac.in

[1] N. W. Ashcroft and N. D. Mermin, Solid State Physics.

[2] K. von Klitzing, G. Dorda, and M. Pepper, Phys. Rev. Lett. **45** 494, (1980).

[3] Topological Insulators: Dirac equation in condensed matter, Springer series in solid state sciences 174.

[4] J. K. Asbóth, L. Oroszlány and A. Pályi, A Short Course on Topological Insulators, arXiv:1509.02295v1.

[5] D. Vanderbilt, Berry Phases in Electronic Structure Theory (Cambridge: Cambridge University Press, 2018).

[6] J. Cayssol and J. N. Fuchs, J. Phys. Mater. **4**, 034007 (2021).

[7] W. P. Su, J. R. Schrieffer, and A. J. Heeger, Solitons in polyacetylene, Phys. Rev. Lett. **42**, 1698 (1979).

[8] J. Zak, Berry's phase for energy bands in solids, Phys. Rev. Lett. **62**, 2747 (1989).

[9] M. V. Berry, Quantal Phase Factors Accompanying Adiabatic Changes, Proc. R. Soc. Lond. A **392**, 45 (1984).

[10] P. Delplace, D. Ullmo, and G. Montambaux, Zak phase and the existence of edge states in graphene, Phys. Rev. B **84**, 195452 (2011).

[11] M. Atala, M. Aidelsburger, J. T. Barreiro, D. Abanin, T. Kitagawa, E. Demler, and I. Bloch, Direct measurement of the zak phase in topological Bloch bands, Nature Physics **9**, 795 (2013).

[12] M. Xiao, Z. Q. Zhang, and C. T. Chan, Surface Impedance and Bulk Band Geometric Phases in One- Dimensional Systems, Phys. Rev. X **4**, 021017 (2014).

[13] W. S. Gao, M. Xiao, C. T. Chan, and W. Y. Tam, Deter- mination of Zak phase by reflection phase in 1D photonic crystals, Opt. Lett. **40**, 5259 (2015).

[14] M. Xiao, G. C. Ma, Z. Y. Yang, P. Sheng, Z. Q. Zhang, and C. T. Chan, Geometric phase and band inversion in periodic acoustic systems, Nat. Phys. **11**, 240 (2015).